Published in final edited form as:

Cancer Discov. 2021 March ; 11(3): 614–625. doi:10.1158/2159-8290.CD-20-0856.

A genetic mouse model recapitulates immune checkpoint inhibitor-associated myocarditis and supports a mechanism-based therapeutic intervention

Spencer C. Wei[1,*], **Wouter C. Meijers**[2,*], **Margaret L. Axelrod**[2], **Nana-Ama A.S. Anang**[1], **Elles M. Screever**[2], **Elizabeth C. Wescott**[4], **Douglas B. Johnson**[2], **Elizabeth Whitley**[3], **Lorenz Lehmann**[6], **Pierre-Yves Courand**[7], **James J. Mancuso**[1], **Lauren E. Himmel**[4], **Benedicte Lebrun-Vignes**[12], **Matthew J. Wleklinski**[2], **Bjorn C. Knollmann**[2], **Jayashree Srinivasan**[5], **Yu Li**[5], **Oluwatomisin T. Atolagbe**[1], **Xiayu Rao**[8], **Yang Zhao**[8], **Jing Wang**[8], **Lauren I.R. Ehrlich**[5,9], **Padmanee Sharma**[10,11], **Joe-Elie Salem**[2,12], **Justin M. Balko**[2,4], **Javid J. Moslehi**[2,#], **James P. Allison**[1,11,#]

[1]Department of Immunology, The University of Texas MD Anderson Cancer Center, Houston, TX, 77030, USA

[2]Department of Medicine, Vanderbilt University Medical Center, Nashville, TN, 37232 USA

[3]Department of Veterinary Medicine and Surgery, The University of Texas MD Anderson Cancer Center, Houston, TX, 77030, USA

[4]Department of Pathology, Microbiology and Immunology, Vanderbilt University Medical Center, Nashville, TN, 37232 USA

[5]Department of Molecular Biosciences, The University of Texas at Austin, Austin TX, 78712 USA

[6]Department of Cardiology, University Hospital of Heidelberg, 69120 Heidelberg, Germany; German Center for Cardiovascular Research (DZHK), partner site Heidelberg/Mannheim; German Research Center (DKFZ), 69120 Heidelberg, Heidelberg

[7]Hospices Civils de Lyon, Service de cardiologie, IMMUCARE, Hôpital de la Croix-Rousse et Hôpital Lyon Sud, Lyon, France; Université de Lyon, CREATIS UMR INSERM U1044, INSA, Lyon France

[8]Department of Bioinformatics and Computational Biology, The University of Texas MD Anderson Cancer Center, Houston, TX, 77030, USA

[9]Livestrong Cancer Institutes, Dell Medical School, The University of Texas at Austin, Austin, TX 78712

Correspondence: Spencer C. Wei, spencer.wei@gmail.com; 510-334-1729, 7455 Fannin St., 1SCR3.1035, Unit 901, Houston, Texas 77054-1901, Javid J. Moslehi, javid.moslehi@vumc.org; 615-343-9436, 2220 Pierce Avenue, 383 PRB, Nashville, TN 37232, or James P. Allison, jallison@mdanderson.org; 713-794-1104, 7455 Fannin St., 1SCR3.1035, Unit 901, Houston, Texas 77054-1901.

*These authors contributed equally

#These authors contributed equally

Author Contributions

S.C.W, J.J.M., and J.P.A. conceived the project and wrote the manuscript. S.C.W., W.C.M., N.A.S.A., Y.Z., X.R., and E.M.W. analyzed data. S.C.W., W.C.M., J.W., J.J.M, and J.P.A. interpreted data.

[10]Department of Genitourinary Medical Oncology, The University of Texas MD Anderson Cancer Center, Houston, TX, USA

[11]Parker Institute for Cancer Immunotherapy, The University of Texas MD Anderson Cancer Center, Houston, TX, 77030, USA

[12]Department of Pharmacology, APHP. Sorbonne Université, INSERM, CIC-1901, UNICO-GRECO Cardio-oncology Program, 75013, Paris, France

Abstract

Immune checkpoint inhibitors (ICI) targeting CTLA-4 or PD-1/PD-L1 have transformed cancer therapy but are associated with immune-related adverse events (irAEs), including myocarditis. Here, we report a robust preclinical mouse model of ICI-associated myocarditis in which mono-allelic loss of *Ctla4* in the context of complete genetic absence of *Pdcd1* leads to premature death in approximately half of mice. Premature death results from myocardial infiltration by T cells and macrophages and severe electrocardiographic abnormalities, closely recapitulating the clinical and pathological hallmarks of ICI-associated myocarditis observed in patients. Using this model, we show that *Ctla4* and *Pdcd1* functionally interact in a gene dosage-dependent manner, providing a mechanism by which myocarditis arises with increased frequency in the setting of combination ICI therapy. We demonstrate that intervention with CTLA-4-Ig (abatacept) is sufficient to ameliorate disease progression and additionally provide a case series of patients in which abatacept mitigates the fulminant course of ICI-myocarditis.

Keywords

CTLA-4; PD-1; *Ctla4*; *Pdcd1*; T cell; negative costimulation; autoimmunity; cardio-oncology; immune-related adverse events; haploinsufficiency; myocarditis

Introduction

Immune checkpoint inhibitors (ICI), including combination therapies such as ipilimumab plus nivolumab, have shown remarkable efficacy across multiple tumor types(1–5) but are associated with immune-related adverse events (irAEs) including myocarditis(6–10). ICI-associated myocarditis is characterized by myocardial T cell and macrophage infiltration, significant electrocardiographic disturbances, with preliminary data suggesting a female predominance, clinically distinguishing it from other forms of myocarditis(7,11,12). ICI-associated myocarditis is also often fulminant and fatal, despite corticosteroid therapy. Therefore, mechanism-based treatment strategies are needed to mitigate serious irAEs such as myocarditis. One major obstacle to improving our understanding of irAEs is the lack of preclinical animal models that recapitulate the clinical course. Herein, we report a murine model that phenotypically recapitulates the clinical pathology of ICI-associated myocarditis and provides mechanistic support for the inhibition of T cell costimulation by CTLA-4-Ig as a treatment for ICI-associated myocarditis.

Results

Combination ICI treatment as the main risk factor for ICI-associated myocarditis

To better define the risk factors for the development of ICI-associated myocarditis, we interrogated VigiBase, WHO's global international pharmacovigilance database of individual case safety reports from January 2008 through June 2019. In comparing myocarditis rates in patients that received monotherapy versus combination ICI therapy, myocarditis was reported at higher frequency for patients treated with combination treatment compared with CTLA-4 or PD-1/PD-L1 therapy alone (84/6858 (1.22%) vs. 329/61192 (0.54%), reporting odds ratio [ROR]: 2.29; 95% confidence interval 1.79–2.91, with n/N being the number of myocarditis case reports over the total number of case reports). Therefore, consistent with previous analyses, the major risk factor associated with development of myocarditis is the combination of CTLA-4 and PD-1 inhibition(13,14).

We assessed whether ICI-associated myocarditis could be recapitulated by pharmacological treatment of a mouse model of autoimmunity. MRL-Fas^{lpr} mice spontaneously develop lupus-like autoimmunity, and loss of PD-L1 in this model leads to autoimmune myocarditis, albeit with a disease pathology driven by antibody deposition that is not observed in patients with ICI-associated myocarditis(15,16). MRL-Fas^{lpr} mice were treated with vehicle, anti-CTLA-4 or anti-PD-1 monotherapy, or combination therapy twice weekly for 8 weeks. Treated mice did not display obvious clinical signs; however, histological and electron microscopic examination revealed subtle immune infiltration of the myocardium and vasculature, as well as signs of endothelial cell damage and sarcomere disarray following combination therapy (Fig. S1A–F). These findings are consistent with increased risk of myocarditis due to combination ICI therapy; but also underscore the absence of preclinical models that recapitulate the disease course of myocarditis associated with ICI therapy, which has been described elsewhere and is notably mechanistically distinct from myocarditis due to other causes (7,14).

Lethal haploinsufficiency of *Ctla4* in the genetic absence of *Pdcd1*

CTLA-4 and PD-1 attenuate T cell activation, but do so through distinct cellular and molecular mechanisms (17–19). Thus, the observed increase in myocarditis rates in combination therapy could either be due to additive effects of two distinct pathologies resulting from manipulation of these biological pathways, or through functional interaction between CTLA-4 and PD-1 which exacerbates the development of this irAE. To distinguish these possibilities, we crossed transgenic mouse strains harboring loss of function alleles of *Ctla4* (encoding CTLA-4) and *Pdcd1* (encoding PD-1) to understand how compound loss of CTLA-4 and PD-1 would affect T cell function and the manifestation of autoimmune pathologies (see Methods) (20,21). Consistent with prior findings, mice with homozygous loss of *Ctla4* succumbed to fatal lymphoproliferative disease with complete penetrance (Fig. 1A) (20,22,23). Approximately 50% of $Ctla4^{+/-}$ $Pdcd1^{-/-}$ mice died by 3 months of age, while littermate controls, including $Ctla4^{+/+}$ $Pdcd1^{-/-}$ mice, remained healthy. This dramatic effect of single copy loss of *Ctla4* in the absence of PD-1 is surprising, given that no haploinsufficiency phenotypes have been previously reported in $Ctla4^{+/-}$ mice with homozygous wild-type *Pdcd1* alleles at either the organismal or cellular level(24),

suggesting that negative regulation by PD-1 is sufficient to buffer against perturbations in T cell signaling caused by heterozygous loss of *Ctla4*. To confirm the mortality observed in *Ctla4*$^{+/-}$ *Pdcd1*$^{-/-}$ mice, we used a second breeding scheme that yields only *Ctla4*$^{+/-}$ *Pdcd1*$^{-/-}$ and *Ctla4*$^{+/+}$ *Pdcd1*$^{-/-}$ littermate mice (Fig. S2A; see Methods) which yielded similar findings with mortality of approximately 50% of *Ctla4*$^{+/-}$ *Pdcd1*$^{-/-}$ mice (Fig. 1B). The incomplete penetrance of mortality raised the possibility that subtle genetic heterogeneity, environmental factors (e.g., microbiome), or stochastic processes influence disease progression. Genetic heterogeneity (e.g., segregating MHC alleles) could not explain the incomplete penetrance of mortality in *Ctla4*$^{+/-}$ *Pdcd1*$^{-/-}$ mice as all tested mice were 97–100% C57BL/6J and no associations between any segregating alleles and clinical signs were observed (Fig. S2B). Similar findings of premature death in *Ctla4*$^{+/-}$ *Pdcd1*$^{-/-}$ mice were observed at a second institution suggesting that environmental factors are not a primary driver of the phenotype (Fig. S2C). The frequency of mortality was partially sex-dependent, with female mice dying at higher frequency than male mice, consistent with the characteristics of ICI-associated myocarditis in patients(11,12) (Fig. 1C). Mortality of *Ctla4*$^{+/-}$ *Pdcd1*$^{-/-}$ mice was often preceded by overt, non-specific clinical signs (*e.g.*, reduced weight gain, reduced movement, dyspnea) beginning as early as 1 month of age. Consistent with *Ctla4* haploinsufficiency in the absence of PD-1, assessment of CTLA-4 protein expression revealed reduced expression levels of total CTLA-4 protein from stimulated T cells derived from lymph nodes from *Ctla4*$^{+/-}$ *Pdcd1*$^{-/-}$ mice (Fig. S2D–S2F) and from those isolated from the thymus (Fig. S3A–S3C).

This indicates that single copy loss of *Ctla4* in the absence of PD-1 results in lowered CTLA-4 levels and raises the possibility that the early mortality of *Ctla4*$^{+/-}$ *Pdcd1*$^{-/-}$ mice arises due to reduced regulatory capacity of CTLA-4 and defects in immunological tolerance. Because *Ctla4* null mice die due to systemic lymphoproliferative disease and *Pdcd1* knockout mice develop mild autoimmunity in specific strains of mice, we explored the possibility that *Ctla4*$^{+/-}$ *Pdcd1*$^{-/-}$ mice develop systemic autoimmunity. No differences in morphology of lymphoid tissues between genotypes were detected in *Ctla4*$^{+/-}$ *Pdcd1*$^{-/-}$ mice (Fig. S4A–F). Furthermore, in contrast to *Ctla4* null mice, *Ctla4*$^{+/-}$ *Pdcd1*$^{-/-}$ mice do not die from uncontrolled lymphoproliferation or a major defect in central tolerance. There was no evidence of systemic organ immune infiltration or elevations in levels of serum cytokines or antibodies (Fig. S5A, S5B). This indicates that *Ctla4*$^{+/-}$ *Pdcd1*$^{-/-}$ mice do not die due to cytokine storm or systemic autoimmunity. However, *Ctla4*$^{+/-}$ *Pdcd1*$^{-/-}$ mice were hypoglycemic and had elevations in serum troponin, a marker of cardiac damage, raising the possibility that cardiac involvement underlies the premature death of *Ctla4*$^{+/-}$ *Pdcd1*$^{-/-}$ mice (Fig. S5C). In a small subset of mice where matched flow cytometry data was also available, elevated troponin was associated with increased cardiac CD45+ immune cell infiltration (Fig. S5D) Comprehensive histologic analysis revealed prominent lymphocytic infiltration in the heart and pancreas of *Ctla4*$^{+/-}$ *Pdcd1*$^{-/-}$ mice (Table S1). Interestingly, histopathologic analysis of other tissues, such as skeletal muscle (Fig. S6A), colon (Fig. S6B), and lung (Fig. S6C) showed minor or no increased immune infiltration in *Ctla4*$^{+/-}$ *Pdcd1*$^{-/-}$ mice compared to *Ctla4*$^{+/+}$ *Pdcd1*$^{-/-}$ mice (Fig. S6D–F), which did not generally result in overt tissue death and was assessed as unlikely to be pathophysiologically relevant. These infiltrations were substantially less pronounced in comparison to the pathologies observed in

the heart and pancreas. Together, these data suggested that *Ctla4*$^{+/-}$ *Pdcd1*$^{-/-}$ mice die due to a breach in peripheral tolerance manifesting in organ-specific autoimmunity.

Myocarditis manifests due to *Ctla4* haploinsufficiency in the absence of *Pdcd1*

Histological examination of the heart tissue indicated dense cellular infiltrates with associated cardiomyocyte necrosis, consistent with myocarditis, in *Ctla4*$^{+/-}$ *Pdcd1*$^{-/-}$ mice. While myocarditis was generally widespread among atrial and ventricular sites, the infiltrates were mostly epicardial and endocardial, consistent with fulminant myocarditis observed in ICI-treated patients (13). Lymphocytic infiltration into the myocardial tissue and myocyte destruction demonstrated patterns similar to those observed in human patients with ICI-induced myocarditis (Fig. 2A). Many of the affected *Ctla4*$^{+/-}$ *Pdcd1*$^{-/-}$ mice displayed evidence of end-stage cardiomyopathy including cardiomegaly, presence of atrial thrombus (Fig. S7A), as well as liver congestion. Other cardiovascular pathological observations included aortic dissection, vasculitis, pulmonary vasculitis, and pericarditis (Fig. S7A). Interestingly, the other site of dramatic lymphocytic inflammation occurred in the exocrine pancreas, with sparing of the islet cells (Fig. S7B). The intensity of the inflammation in *Ctla4*$^{+/-}$ *Pdcd1*$^{-/-}$ mice varied, consistent with the incomplete penetrance of mortality. These pathological abnormalities were not observed in *Ctla4*$^{+/+}$ *Pdcd1*$^{-/-}$ mice, underscoring the critical importance of *Ctla4* in disease pathogenesis. More minor inflammation was observed in other organs of both *Ctla4*$^{+/-}$ *Pdcd1*$^{-/-}$ and *Ctla4*$^{+/+}$ *Pdcd1*$^{-/-}$ mice, consistent with autoimmunity observed upon loss of PD-1 (21,25,26). Lymphocytic infiltration consisted of CD3+ CD8+ T cells, and CD4+ T cells to a lesser abundance in *Ctla4*$^{+/-}$ *Pdcd1*$^{-/-}$ mice, mirroring observations in patients(7) (Fig. 2B–C). In agreement with phenotypic observations, histopathology scores of cardiac H&E sections in *Ctla4*$^{+/-}$ *Pdcd1*$^{-/-}$ demonstrated increased prevalence of myocarditis with high CD3+ lymphocytic infiltrate, high F4/80+ macrophage infiltrate, and low Foxp3+ regulatory T cell abundance (Fig. 2D). Increased PD-L1 expression was also observed in cardiac tissue of *Ctla4*$^{+/-}$ *Pdcd1*$^{-/-}$ mice similar to prior clinical observations (Fig. S7C–D)(7). We further characterized cellular infiltrates in female 3–6 week old *Ctla4*$^{+/-}$ *Pdcd1*$^{-/-}$ and *Ctla4*$^{+/+}$ *Pdcd1*$^{-/-}$ mice by flow cytometry. Increased frequencies of total CD45^{+} immune cells, CD8+ T cells, and CD68+ macrophages were observed in *Ctla4*$^{+/-}$ *Pdcd1*$^{-/-}$ mice compared to littermate *Ctla4*$^{+/+}$ *Pdcd1*$^{-/-}$ mice (Fig. 2E, Fig. S8, Fig. S9A). In contrast, no difference was observed in matched splenic populations (Fig. S9B). Mice were highly heterogenous in levels of infiltrate, consistent with the heterogeneity and incomplete penetrance observed at the phenotypic level. Given these observations, we then tested whether the disease pathogenesis of *Ctla4*$^{+/-}$ *Pdcd1*$^{-/-}$ mice is immune mediated. Premature mortality appeared to be attenuated in *Ctla4*$^{+/-}$ *Pdcd1*$^{-/-}$ *Rag1*$^{-/-}$ mice compared to littermate *Ctla4*$^{+/-}$ *Pdcd1*$^{-/-}$ *Rag1* competent mice (Fig. 2F, Fig. S9C). Although this comparison did not meet statistical significance (potentially due to the impact of *Rag1*$^{-/-}$ immunodeficiency independent of myocarditis, evidenced by premature deaths observed in *Ctla4*$^{+/-}$ *Pdcd1*$^{+/-}$ *Rag1*$^{-/-}$ mice), it is consistent with a role for adaptive immunity in disease pathogenesis.

Cardiac alterations in *Ctla4*$^{+/-}$ *Pdcd1*$^{-/-}$ mice reflect the clinical course of checkpoint blockade-associated autoimmune myocarditis

To further characterize clinical cardiac disease, we performed extensive cardiovascular and physiological examination in all *Ctla4*$^{+/-}$ *Pdcd1*$^{-/-}$ and littermate *Ctla4*$^{+/+}$ *Pdcd1*$^{-/-}$ mice. Considerable heterogeneity was observed in echocardiographic parameters of *Ctla4*$^{+/-}$ *Pdcd1*$^{-/-}$ mice compared to *Ctla4*$^{+/+}$ *Pdcd1*$^{-/-}$ mice such that no statistically significant differences were observed. However, stratification of mice based on immune infiltrates revealed an association between increased immune infiltration and cardiomegaly as manifested by increased heart weight to body weight ratio and ventricular wall thickening on echocardiography without systolic cardiac dysfunction (Fig. 3A–B). Detailed electrocardiographic (ECG) examination revealed significant arrhythmogenic disturbances including sinus node dysfunction, sinus arrest and atrioventricular conduction block and severe bradycardia in *Ctla4*$^{+/-}$ *Pdcd1*$^{-/-}$ mice, but not *Ctla4*$^{+/+}$ *Pdcd1*$^{-/-}$ mice (Fig. 3C–3E), consistent with arrhythmogenic nature of ICI-myocarditis in patients(7) (Fig. 3F). The pattern of myocarditis and electrocardiographic instability observed in these mice are consistent with clinical observations from patients with ICI-associated myocarditis(7,27,28).

Therapeutic intervention with CTLA-4-Ig rescues the fatal myocarditis that arises in *Ctla4*$^{+/-}$ *Pdcd1*$^{-/-}$ mice

The development of a robust mouse model of ICI-associated myocarditis enables testing of therapeutic regimens. Our finding that the development of myocarditis is gene dosage-dependent raises the hypothesis that restoration of CTLA-4 and/or PD-1 signaling would be sufficient to prevent disease progression. To test this hypothesis, 3-week-old *Ctla4*$^{+/-}$ *Pdcd1*$^{-/-}$ mice were treated with vehicle or abatacept (recombinant CTLA-4 Ig) to block T cell costimulation by binding to B7 ligands, prior to the development of any overt clinical signs. Abatacept treatment significantly reduced mortality of *Ctla4*$^{+/-}$ *Pdcd1*$^{-/-}$ mice (Figure 4A). At a cellular level, abatacept did not decrease myocardial immune infiltrates at 2 weeks; however, after 14 weeks, immune infiltrates in the heart returned to near-baseline levels (Fig. 4B). In an effort to identify biomarkers associated with disease progression or response, we assessed heart weight-body weight ratios. No statistically significant difference was observed between genotypes; however, decreased cardiomegaly was observed following abatacept treatment (Fig. 4C). These observations provide preclinical rationale for further investigation of CTLA-4-Ig as a treatment for autoimmune irAEs associated with ICI therapy. Clinically, we have previously published a case report of a corticosteroid-refractory ICI-myocarditis successfully treated with abatacept (29), and provide clinical details on two additional similarly-responding ICI-myocarditis patients in which abatacept led to amelioration of the clinical features of myocarditis (Table S2 and Fig. S10). Thus, preliminary evidence exists that response to CTLA-4-Ig in this model seems to replicate that observed in clinical patients, though more investigation is clearly needed. Nonetheless, these data further support the mechanistic basis for the ability of CTLA-4-Ig intervention to attenuate autoimmunity caused by either anti-PD-1 monotherapy or combination anti-CTLA-4 plus anti-PD-1 treatment.

Discussion

Here we identify gene dosage-dependent genetic and functional interaction between the T cell negative costimulatory genes *Ctla4* and *Pdcd1*, which manifests as fatal myocarditis in *Ctla4*$^{+/-}$ *Pdcd1*$^{-/-}$ mice, providing a robust genetic mouse model for myocarditis and other cardiovascular toxicities associated with CTLA-4 and PD-1 ICI therapy. This model addresses a key limitation in the field and enables mechanistic investigation of ICI-induced irAEs. Importantly, this mouse strain models myocarditis associated with monotherapy and combination ICI therapy, which are both fundamentally driven by aberrant T cell activation. In patients most T cells are antigen experienced whereas most T cells in laboratory mice are naïve, which explains why PD-1 blockade can lead to myocarditis in humans but additional perturbations are required in mice. Specifically, naïve T cells require CD28 costimulation to activate (which will not normally be provided for self-antigens), while in contrast the activity of antigen experienced cells can be enhanced by PD-1 blockade alone. Dual PD-1 and CTLA-4 blockade enhances both of these processes, providing mechanistic rationale for the association with a higher frequency of myocarditis. Fundamentally, these data support a threshold model of T cell activation in which CTLA-4 and PD-1 regulatory signals functionally integrate to provide a critical buffering system to restrain T cell activation. Gene dosage of *Ctla4* and *Pdcd1* together define the functional threshold of T cell self-recognition. These findings are consistent with the understanding that CTLA-4 and PD-1 attenuate T cell activation through distinct cellular and molecular mechanisms (17–19), provide mechanistic insights into how ICI-associated myocarditis arises, and present a preclinical model to test therapeutic interventions to mitigate irAEs.

Based on the functional interaction between CTLA-4 and PD-1, intervention with CTLA-4-Ig, which blocks T cell costimulation, may be an effective therapeutic intervention for myocarditis associated with monotherapy and combination ICI therapy – a provocative possibility that is supported by preliminary clinical reports and warrants future prospective clinical testing. However, the effect of CTLA-4-Ig treatment on tumor growth must be fully understood, particularly given that CD28 signaling is required for T cell priming and for responses to checkpoint blockade(17,18,30). It is tempting to speculate that CTLA-4-Ig could be administered after the initial priming of tumor-reactive T cells, allowing anti-tumor responses to be maintained; however, this possibility requires investigation.

Critical open questions remain, including how ICI efficacy and irAEs are related, how irAEs may be mitigated, and in what contexts ICI therapy is warranted. Our results reveal a functional interaction between CTLA-4 and PD-1, with particular relevance to cardiovascular homeostasis. While mice heterozygous for *Ctla4* appear normal, complete loss of CTLA-4 leads to unrestrained fatal lymphoproliferation; however, the inflammation is not specific to the cardiovascular system in these models. On the other hand, the phenotype of *Pdcd1*$^{-/-}$ mice is dependent on genetic background. While PD-1 loss in a C57BL/6 strain does not result in significant cardiovascular toxicity, BALB/c mice deficient for PD-1 display autoantibody-mediated cardiomyopathy upon aging (25,26,31). However, this model does not recapitulate ICI-myocarditis in humans clinically or pathologically. On the other hand, the disease etiology of *Ctla4*$^{+/-}$ *Pdcd1*$^{-/-}$ mice closely recapitulates ICI-associated myocarditis. The sex imbalance seen in our mice is consistent with emerging data

from patients where female sex is associated with increased risk of irAEs and myocarditis specifically (11,12). These early observations in ICI-myocarditis are in contrast with general myocarditis which appears to occur with higher frequency in men (32).

From a perspective of basic T cell biology, the precise molecular and cellular mechanism by which CTLA-4 and PD-1 functionally interact remains unclear. These data further support a threshold model of T cell costimulation, in which loss of PD-1 and CTLA-4 lead to a decreased threshold for T cell activation and enables aberrant activation of self-reactive T cells. The manifestation of severe autoimmunity in specific tissues in this model and individual patients receiving ICIs may reflect one or more potential mechanisms including the predisposition of particular antigens to autoimmune recognition in the absence of negative costimulation, functional differences between tissue-specific T_{reg} populations(33), or environmental factors.

Our findings also raise the possibility that subtle changes in gene dosage of *CTLA4* and *PDCD1* may predispose some patients to the development of cardiovascular irAEs. Heterozygous germline loss of function alleles of *CTLA4* in humans leads to immune dysregulation with highly variable clinical presentation and incomplete penetrance(34–36). Our preclinical data provide biological rationale and support further investigation of CTLA-4-Ig as a potential therapy for ICI-induced autoimmune irAEs. Our results are further supported by preliminary patient data whereby treatment with abatacept attenuated cases of steroid-refractory ICI-associated myocarditis. Although there was no evidence of tumor growth due to abatacept treatment in the small sample of patients that we had, longer follow-up and more patient cases are needed. Further data are needed to understand the effects of abatacept on tumor growth in preclinical and clinical settings. These clinical data are provocative but preliminary, but they support the pivotal importance of manipulating T cell costimulation for the treatment of ICI-myocarditis and the need for prospective interventional trials with abatacept for ICI-associated myocarditis, where both cardiovascular endpoints, as well as cancer endpoints would be assessed.

Methods and Materials

Mice

Ctla4^{tm1All} mice(20) were bred to *Pdcd1* knockout mice (*Pdcd1*$^{tm1.1Shr}$)(21), which were purchased from The Jackson Laboratory (021157). *Pdcd1* knockout mice were backcrossed once to C57BL/6J, prior to breeding crosses with *Ctla4* mice. We first used a heterozygous intercross-breeding scheme using *Ctla4*- and *Pdcd1*-knockout transgenic mice (Fig. S1A) to allow for the generation of all possible permutations of mutant alleles from a single cross and for estimation of the observed recombination frequency between *Ctla4* and *Pdcd1*. This first breeding scheme specifically utilized F1 mice derived from the cross of *Ctla4*$^{+/-}$ (which are wild-type for *Pdcd1*) and *Pdcd1*$^{-/-}$ mice (which are wild-type for *Ctla4*). This is important, because this breeding scheme ensures that mutant alleles of *Ctla4* and *Pdcd1* in F1 mice are in *trans*, and thus the recombination frequency can be calculated. We observed a recombination frequency of 17.03 cM between the murine *Ctla4* and *Pdcd1* loci, consistent with the 16.89 cM distance estimate by the Mouse Phenome Database (MPD,

RRID:SCR_003212)(37). The genetic distance between *Ctla4* and *Pdcd1* was calculated by assessing the number of recombination and total events in this cross.

To verify findings from the first breeding scheme, a second related breeding scheme was utilized (Fig. S1A). Importantly, this breeding approach utilized different genotypes, the mutant alleles could either be in *cis* or in *trans*, and would generate *Ctla4*$^{+/-}$ *Pdcd1*$^{-/-}$ (experimental) and *Ctla4*$^{+/+}$ *Pdcd1*$^{-/-}$ (control littermates) in a 1:1 ratio. This allows for the generation of many more *Ctla4*$^{+/-}$ *Pdcd1*$^{-/-}$ mice than in the initial breeding approach. Specifically, male *Ctla4*$^{+/-}$ *Pdcd1*$^{-/-}$ and female *Ctla4*$^{+/+}$ *Pdcd1*$^{-/-}$ were bred. Female *Ctla4*$^{+/+}$ *Pdcd1*$^{-/-}$ were used to eliminate the possibility that the autoimmunity or other phenotypes observed in *Ctla4*$^{-/+}$ *Pdcd1*$^{-/-}$ might affect fetal-maternal tolerance or the ability to produce viable litters.

For the generation of survival curves, events were defined as either death (i.e. mice found dead) or identification of mice by veterinary staff as requiring euthanasia (e.g. due to lethargy, moribund, dyspnea). For mice identified as required euthanasia, the date of death was defined as the day the mouse was identified by veterinary staff. Animal phenotypes associated with mortality were identified and reported by veterinary staff. Mice utilized for breeding or other analyses (e.g., histological examination) were included in survival analyses in addition to initial cohorts primarily dedicated to assessing survival. Mice were censored from survival analyses at the time they were utilized for alternative purposes or analyses. Survival analyses of *Ctla4*$^{+/-}$ *Pdcd1*$^{-/-}$ *Rag1*$^{-/-}$ and littermate *Rag1* competent mice were described as above. Notably as a caveat of these specific analyses, because *Ctla4*$^{+/-}$ *Pdcd1*$^{-/-}$ *Rag1*$^{-/-}$ mice are the only immunodeficient genotype within the groups expected to develop fatal myocarditis (i.e., *Ctla4*$^{+/-}$ *Pdcd1*$^{-/-}$ groups), premature deaths in this genotype can be attributed to either causes associated solely with immunodeficiency (e.g., infection) or incomplete rescue of autoimmune phenotypes (e.g., myocarditis) by loss of adaptive immunity. Analysis of female mice in which the premature death is more penetrant, provided further support for the former possibility (Fig. S9C).

All mice were housed at The University of Texas MD Anderson Cancer Center South Campus Vivarium, an AAALAC-accredited, specific pathogen free (SPF) animal facility, or at the Vanderbilt University Medical Center, also an AAALAC-accredited, SPF animal facility. Given that the vivaria are SPF and not germ free, it is presumed that untested infectious agents may be present and it is possible that they could modulate the manifestation of disease. All experiments were performed in accordance with The University of Texas MD Anderson Cancer Center Institutional Animal Care and Use Committee (IACUC) guidelines or the Vanderbilt University Medical Center IACUC guidelines.

Genotyping

Genomic DNA was isolated using DirectPCR Lysis Reagent (Viagen Biotech, 101-T) supplemented with Proteinase K. Polymerase chain reaction (PCR) based genotyping using crude lysate was performed for *Ctla4* and *Pdcd1* knockout mice. *Ctla4*^{tm1All} mice were genotyped as previously described(20). The expected band sizes for the *Ctla4* wild-type and mutant alleles are ~75 and ~150 bp, respectively. *Pdcd1* knockout mice were genotyped as

previously described(21). The expected band sizes for the *Pdcd1* wild-type and mutant alleles are 418 and 350 bp, respectively. *Ctla4* primers: 5' AAACAACCCCAAGCTAACTGCGACAAGG 3', 5' CCAGAACCATGCCCGGATTCTGACTTC 3', 5' CCAAGTGCCCAGCGGGGCTGCTAAA 3'. *Pdcd1* primers: PD1 KO common 24743 (5' CACTATCCCACTGACCCTTCA), PD1 KO WT rev (5' AGAAGGTGAGGGACCTCCAG), and PD1 KO Mut rev (5' CACAGGGTAGGCATGTAGCA).

SNP typing

Crude genomic DNA lysate was submitted to The University of Texas MD Anderson Cancer Center Laboratory Animal Genetics Services core facility for SNP typing using a 100-marker panel. *Ctla4*$^{-/+}$ *Pdcd1*$^{-/-}$ mice derived from both the first and second (validation) breeding schemes were analyzed. For the purpose of determining whether genetic variants associate with autoimmunity, 'unaffected' (defined as no observable clinical symptoms within the 6 months of age) and 'affected' (defined as mice that died or were identified as requiring euthanasia) *Ctla4*$^{-/+}$ *Pdcd1*$^{-/-}$ mice were compared. 129 (the original derivation strain) and B6 SNPs were assessed to test for association with phenotypic outcomes.

Pathology

Animal necropsies were performed by personnel in The University of Texas MD Anderson Cancer Center veterinary medical histology laboratory, in the Allison laboratory, or at Vanderbilt University Medical Center. Automated serum chemistry analysis using a Cobas Integra 400Plus (Roche Diagnostics, Risch-Rotkreuz, Switzerland) was performed on a blood sample collected at euthanasia. Formalin-fixed tissues were processed routinely into paraffin blocks, sectioned at 5 microns, and stained with hematoxylin and eosin. Additional sections were used for immunohistochemical (IHC) staining of particular tissues of interest, using an antibody directed against CD3 (ab16669, Abcam, Cambridge, MA), CD4 (25229, Cell Signaling Technologies), CD8a (98941, Cell Signaling Technologies), F4/80 (ab100790, Abcam), or FoxP3 (12653, Cell Signaling Technologies), followed by secondary reagents for chromogenic detection (Bond Polymer Refine Detection system, DS9800, Leica, Buffalo Grove, IL). Stained sections were examined using a Leica DM2500 microscope with Leica DFC495 camera and Leica Application Suite v4.12 software.

Slides preparation at Vanderbilt University Medical Center:

Formalin-fixed tissues were routinely processed, cut at 4–5 microns, and stained with hematoxylin and eosin by standard protocols in Vanderbilt University Medical Center's Translational Pathology Shared Resource core laboratory. To further characterize the mononuclear cardiac infiltrates detected by light microscopy, a panel of immunohistochemical (IHC) markers was employed. IHC staining was performed in the TPSR using standard, validated protocols for chromogenic IHC. All steps besides dehydration, clearing and coverslipping were performed on the Leica Bond-Max IHC autostainer (Leica Biosystems Inc., Buffalo Grove, IL). Slides were deparaffinized. Antigen retrieval was performed using EDTA (CD markers) or proteinase K (F4/80). Slides were incubated with primary antibodies as indicated below. Secondary antibody labeling was

performed for all markers except CD3 by incubating in rabbit anti-rat antibody (BA-4001, Vector Laboratories, Inc., Burlingame, CA) for 15 minutes at a 1:650 dilution. Immunolabeling by rabbit antibody was visualized using the Bond polymer refine detection system (#DS9800, Leica Biosystems, Inc.). Slides were then dehydrated, cleared and coverslipped. For primary antibodies, anti-CD45R (BD Biosciences, RA3–6B2) was used at 1:20,000 dilution as a B cell marker, anti-CD3 (Abcam, Ab16669) was used at 1:250 dilution as a pan-T cell marker, anti-CD4 (eBioscience, 14–9766-82) was used at 1:1000 dilution as a Th cell marker, anti-CD8 (eBioscience, 14–0808-82) was used at 1:1000 dilution as Tc cell marker, and anti-F4/80 (Novus Biologicals, NB600–404) was used at 1:900 dilution as macrophage marker.

Histologic Scoring: Microscopic analysis and semi-quantitative scoring of morphologic lesions was conducted by two board-certified veterinary anatomic pathologists, one of whom was blinded to the mouse genotypes/treatments. Semi-quantitative scoring was performed to characterize the magnitude of myocardial infiltrates in 6 distinct cardiac regions: ventricular endocardium, ventricular myocardium and perivascular adventitia, ventricular epicardium, atria, aorta, and pericardium. The sum of scores assigned for all regions was calculated for each mouse for a composite score, and group means of the composite scores are presented. Scores were performed as follows: 0 – Within normal limits; 1 - minimal <10% affected; 2 – mild, 10–20% affected; 3 – moderate, 20–50% affected, 4 – marked, >50% affected.

Histopathology: image analysis—Image analysis was conducted by a board-certified veterinary anatomic pathologist under masked conditions. Heart sections from the same mice evaluated by H&E and immunophenotyping were analyzed. Slide scanning was performed on the Pannoramic 250 Flash III digital scanner (3DHISTECH Ltd., Budapest, Hungary). Quantification of immunolabeled cells in the hearts was performed in QuPath version 0.2.0-m4, an open source digital pathology platform (38), using manual region of interest delineation of the atria and ventricles and a single-threshold positive cell detection feature. Data were collected per heart section and then group-wide means of percentage of positive CD3, CD4, and CD8 cells were calculated. Parameters were set up as follows: detection image: hematoxylin OD, pixel size: 0.5 μm, nucleus – background radius: 8 μm, nucleus – median filter radius: 0 μm, nucleus – sigma: 1.2 μm, nucleus – min area: 10 μm^2, nucleus – max area: 400 μm^2, intensity – threshold: 0.1, max background intensity: 2, intensity: split by shape, cell expansion: 4 μm, cell parameter: include cell nucleus, boundaries: smooth boundaries, measurements: make measurements, score compartment: nucleus – DAB OD mean, threshold 1+: 0.2.

Cardiac dissociation and flow cytometry

Single cell suspensions were obtained from hearts of 3–6 week old female wild-type, *Ctla4*$^{+/+}$ *Pdcd1*$^{-/-}$ or *Ctla4*$^{+/-}$ *Pdcd1*$^{-/-}$ mice by mincing followed by enzymatic digestion with 125U/mL DNase I (Worthington cat no. LS002138) and 250U/mL Collagenase 3 (Worthington cat no.LS004182). Dissociated hearts were filtered through a 70uM filter. Red blood cells were lysed using ACK lysing buffer (KD Medical/MediaTech cat no. NC0274127). Cells were washed with PBS and stained for flow cytometry. Cells were first stained with Zombie Violet fixable viability dye for 20 minutes at room temperature,

followed by Fc block (TruStain FcX™ (anti-mouse CD16/32) Antibody; BioLegend cat no. 101320) for 5 minutes at 4°C. Cells were washed and stained with surface stain for 20 minutes at 4°C, as indicated below. Cells were then fixed with either eBioscience Fix/Perm (Thermo Fisher cat no. 88–8824-00) kit for cytoplasmic antigens (*i.e.* CD68) or True-Nuclear™ Transcription Factor Buffer Set (BioLegend cat no. 424401) for nuclear antigens (*i.e.* FoxP3). Samples were run on an Attune NxT Acoustic Focusing Cytometer. Analysis was performed in FlowJo, using two different panels of antibodies on the same sample. Gating was first done on forward scatter (FSC) and side scatter to exclude debris. Doublets were excluded by gating on FSC-area vs. FSC-height. Given massive cell death in the cardiomyocytes, percentages were calculated out of total cardiac single cells. Next, viable (zombie violet negative) immune cells (CD45+) were gated and used for all downstream immune cell gates. T cells were defined as CD3+ and gated into CD3+CD4+CD8- or CD3+CD8+CD4-. Tregs were defined as CD3+CD4+CD8-FoxP3+. Macrophages were defined as CD68+. Natural killer/ NK-T cells were defined as CD68-NK1.1+. B cells were defined as CD68-CD19+. CD68-CD11c+ cells are also enumerated, which are primarily comprised of dendritic cells. Zombie Violet (cat no. 423114), PerCP/Cy5.5 anti-mouse CD45 (clone 30-F11, cat no. 103132), Alexa Flour 488 anti-mouse CD3 (clone 17A2, cat no. 100210), APC anti-mouse CD4 (clone GK1.5, cat no. 100412), PE/Cy7 anti-mouse CD8a (clone 53–6.7, cat no. 100722), APC/Cy7 anti-mouse CD19 (clone 6D5, cat no. 115530), Alexa Flour 488 anti-mouse CD11c (clone N418, cat no. 117311), PE/Cy7 anti-mouse IA/IE (clone M5/114.15.2, cat no. 107630), PE anti-mouse CD68 (clone FA-11, cat no. 137013), APC anti-mouse NK1.1 (clone PK136, cat no. 108710), and APC/Cy7 anti-mouse CD11b (clone M1/70, cat no. 101225) were purchased from BioLegend. PE anti-mouse FoxP3 (clone FJK-16s, cat no. 101225) was purchased from Thermo Fisher.

T cell restimulation and flow cytometry

Single cell suspensions from lymph nodes were prepared by mashing pooled inguinal, axillary, and brachial lymph nodes through a 70um filter using the back of a plastic syringe into RPMI-1640 supplemented with 10% FBS and 1% Penicillin Streptomycin. A 96-well flat bottom plate was coated 200ul per well of 1ug/ml anti-CD3e and 2ug/ml anti-CD28 in PBS overnight at 4ºC the previous night. Cells were then stained with CellTrace Violet Proliferation kit per the manufactures protocol (Invitrogen, C34557). Triplicates of each sample were plated 10^6 cells/mL per well in 200ul of RPMI-1640 supplemented with 10% FBS, sodium pyruvate, 0.1% b-ME, and P/S and incubated at 37°C for 46 hours. Cells were then transferred to a U-bottom 96-well plate and washed twice with FACS buffer and incubated with 2% of each bovine, murine, rat, hamster, and rabbit serum PBS with 25 mg/mL 2.4G2 antibody at 4°C for 10 min prior to surface staining with an antibody cocktail at 4°C for 30 min in a 50 uL volume. Cells were washed twice with FACS buffer then fixed and permeabilized using the FoxP3 fix and permeabilization kit according to manufacturer's protocol (eBioscience). Cells were subsequently stained with an intracellular antibody cocktail at room temperature for 30 min. Cells were then washed twice with Foxp3 permeabilization buffer, then twice with FACS buffer, and analyzed on a LSRII (BD). PE mean fluorescence intensity (MFI) was then quantified to assess CTLA-4 protein levels in T cells from mice.

Surface stain (restim): LIVE/DEAD™ Fixable Blue Dead Cell Stain (cat no. L23105) was purchased from Thermo Fisher. BV786 Hamster Anti-Mouse CD3e (clone 145–2C11, cat no. 564379) was purchased from BD. Brilliant Violet 605 anti-mouse TCR β chain antibody (clone H57–597, cat no. 109241), Brilliant Violet 650 anti-mouse CD19 antibody (clone 6D5, cat no. 115541), PE anti-mouse CD152 antibody (clone UC10–4B9, cat no. 106306), and PE Armenian Hamster IgG Isotype Ctrl antibody (clone HTK888, cat no. 400908) were purchased from BioLegend. FITC Anti-mouse CD4 Antibody (clone RM4.5, cat no. 11–0042-82), APC Anti-mouse CD8a Antibody (clone 53–6.7, cat no. 17–0081-82), and Alexa Fluor 700 Anti-mouse CD45.2 Antibody (clone 104, cat no. 56–0454-82) were purchased from ebio.

IC stain (restim): BV786 Hamster Anti-Mouse CD3e (clone 145–2C11, cat no. 564379), Brilliant Violet 605 anti-mouse TCR β chain antibody (clone H57–597, cat no. 109241), PE anti-mouse CD152 (CTLA-4) Antibody (clone UC10–4B9, cat no. 106306), and PE Armenian Hamster IgG Isotype CTLA-4 Ctrl antibody (clone HTK888, cat no. 400908) were purchased from BioLegend. FITC Anti-mouse CD4 Antibody (clone RM4.5, cat no. 11–0042-82) and APC Anti-mouse CD8a Antibody (clone 53–6.7, cat no. 17–0081-82) were purchased from ebio.

Pharmacological Model

Female MRL/MpJ-Fas/lpr mice were purchased from Jackson Laboratories at 3–4 weeks. After 1 week of acclimatization, mice were treated with anti-CTLA4, anti-PD-1 antibody (Thermo Fisher Scientific, both 200 ug), anti-PD-1 (ThermoFisher Scientific, 200 ug), both or vehicle. Immunofluorescence staining of cardiac tissues was performed at Vanderbilt University using anti-CD3 (Novus) and anti-CD68 (Novus) antibodies, as described above.

Abatacept injection

Mice were injected intraperitoneally with either 100ul PBS with 200ug CTLA-4 Ig (Abatacept, purchased from Vanderbilt pharmacy) or vehicle, three times a week, for up to 80 days, starting at 21 days of age. Although abatacept is a human CTLA-4-Ig fusion, it also functions in mouse models due to the high similarity between human and mouse CTLA-4 (39).

Electrocardiography (ECG) in anesthetized mice

ECG records were created in the different genetic models to assess presence of arrhythmogenic disturbances. Once mice were anesthetized with 3% isoflurane inhalation, needle electrodes where placed subcutaneously into all four limbs. Isoflurane was then lowered to 1% to maintain stable sedation and ECG recording was started. ECG traces were recorded for 4–5 minutes. ECG analysis was conducted in LabChart 8 by two observers blinded to the genotype and then compared for precision. Conduction disturbances were quantified as the number of mice in each group as percentage. ECG records were reviewed and ventricular ectopic beats (VEB) identified based on standard criteria (i.e., wide QRS complex, AV dissociation).

Echocardiogram in un-anesthetized mice

Before sacrifice, *in vivo* cardiac dimensions were assessed with M-mode and 2D transthoracic echocardiography (Vevo 2100; Fujifilm VisualSonics, Toronto, Canada). Mice were not anesthetized during echocardiography. Parasternal long axis views were used to record M-mode tracings at left ventricular mid-papillary level to measure left ventricular dimensions (interventricular septum (IVS), left ventricular posterior wall (LVPW), left ventricular internal diameter (LVID) and % ejection fraction (EF)).

Luminex cytokine and chemokine assessment

Serum was collected from *Ctla4*$^{+/-}$ *Pdcd1*$^{-/-}$ and control littermate mice (including both *Ctla4*$^{+/+}$ *Pdcd1*$^{-/-}$ mice and mice competent for both CTLA-4 and PD-1 such as *Ctla4*$^{+/-}$ *Pdcd1*$^{+/-}$ mice) from both breeding schemes described above. Briefly, blood was collected by terminal cardiac puncture after deep anesthesia was established during CO2 euthanasia. Blood was allowed to coagulate at room temperature, centrifuged at 2,000g for 10 minutes, supernatant serum collected, snap frozen in liquid nitrogen, and stored at −80 degrees Celsius for later analysis. Serum levels of antibodies cytokine and chemokine were assessed using the Cytokine & Chemokine 36-plex Mouse ProcartPlex luminex assay (ThermoFisher Scientific) per manufacturer's protocol. All samples were analyzed in parallel in a single batch for each respective analysis. Serum samples were diluted 1:10,000 for analysis of serum antibody levels. Cardiac TnI concentration in serum was measured by a mouse-specific ELISA (Cat# 2010–1-HSP, Life Diagnostics, Inc., West Chester, PA). Standard and sample volumes were reduced to 25 μL from the manufacturer's recommended 100 μL per well to conserve limited sample volume.

Messenger RNA Analysis

Messenger RNA (mRNA) was purified with TRIzol (Invitrogen, Carlsbad, Calif) and RNeasy column (Qiagen, Valencia, Calif). Total RNA (0.5 microgram) was reverse transcribed (StrataScript First Strand cDNA Synthesis Kit; Stratagene, La Jolla, Calif) and analyzed by real-time PCR using RT2 Profiler PCR Arrays (SABiosciences, Frederick, Md) and Mx3005 thermocycler (Stratagene). The following primers were used for the *cd274* (PD-L1) mRNA: 5'-TGCGGACTACAAGCGAATCACG-3', 3'-CTCAGCTTCTGGATAACCCTCG-5'; 5'-GCTCCAAAGGACTTGTACGTG-3', 3'-GCTCCAAAGGACTTGTACGTG-5'.

Immunohistochemistry

Paraffin-embedded tissue sections were immunostained for PDL1 using a murine PD-L1 antibody (Cell Signaling, Danvers, MA) at 1:75 dilution.

Transmission Electron Microscopy

Hearts were fix perfused with ice-cold buffer containing 2.5% paraformaldehyde, 2.5% glutaraldehyde, and 0.1 mol/L sodium cacodylate (pH 7.4) (No. 15949; Electron Microscopy Sciences, Hatfield, Pa). Heart tissues from the endocardial aspect of the LV wall were embedded for transmission electron microscopy (Tecnai G2 Spirit BioTWIN; FEI Co, Hillsboro, Ore) with a cooled charge coupled device camera (XR41C; Advanced

Microscopy Techniques, Danvers, Mass) and Image Caption Engine acquisition software (Advanced Microscopy Techniques).

VigiBase Analysis

PD1 inhibitors considered for disproportionality analysis in VigiBase were nivolumab, pembrolizumab and cemiplimab. PD-L1 inhibitors considered for this analysis were atezolizumab, durvalumab, and avelumab and CTLA-4 inhibitor was ipilimumab. Methods utilized as previously described (14,40). Myocarditis (n:413) was identified as reporting (Autoimmune myocarditis and/or Myocarditis; preferred term levels of Medical Dictionary for Regulatory Activities) in patients who received combination ICI targeting CTLA-4 and PD-1/PD-L1 (e.g, ipilimumab and nivolumab) compared to single CTLA-4 or PD-1/PD-L1 therapy. With VigiBase (N=16,337,777 reports since 01/2008), reporting odds ratio (ROR) allows comparisons across toxicities and drug groups.

Statistics

Statistical analyses were performed in Prism 7.0 or 8.0 (GraphPad Software, San Diego, CA), unless otherwise noted.

Data and code availability

Publicly available data was obtained from VigiBase (https://www.who-umc.org/vigibase/vigibase/). All other data are available upon request from the authors after appropriate approvals.

Human research ethics

All evaluation of clinical data on adverse drug reactions from multisource databases and real world signal detection was performed under ethics guidelines established by and with the approval of the Vanderbilt University Medical Center Human Research Protections Program and Institutional Review Board (IRB # 181337), who determined that the work did not meet the definition of human subject research. No identifiable private information was obtained by the research team.

Supplementary Material

Refer to Web version on PubMed Central for supplementary material.

Acknowledgments

We acknowledge the contributions of Mary Barber and Gosife D. Okoye and Elie Tannous for the early parts of this project as well as Drs. Maël Richard, Anissa Bourli, Brahim Harbaoui, Raphaele Nove-Josserand, Julien Peron, Tanguy Fenouil, Pierre Lanteleme. This work was supported by a grant from Cancer Prevention and Research in Texas to J.P.A. (R1203) and NCI Cancer Center Support Grant (CCSG) P30CA16672 which supports core facilities at MD Anderson Cancer Center including the Reverse Phase Proteomic array, Veterinary Pathology, Laboratory Animal Genetics, and Statistical support cores that were utilized in the described work, as well as NCI/NIH Cancer Center Support Grant 5P30 CA68485-19 (to Vanderbilt) and the Vanderbilt Mouse Metabolic Phenotyping Center Grant 2 U24 DK059637-16. JJM was supported by NIH grants – R56 141466 and R01 141466. DBJ and JMB were supported by NCI/NIH R01CA227481. Additional funding was provided by NIH T32GM007347 (MLA) and F30CA236157 (MLA). S.C.W. was a MD Anderson Cancer Center Odyssey postdoctoral fellow and is currently an employee of Spotlight Therapeutics. J.P.A. is a CPRIT Scholar in Cancer Research and a Director of the Parker Institute for Cancer Immunotherapy. The supplied data from VigiBase come from various sources. The likelihood

of a causal relationship is not the same in all reports. The information does not represent the opinion of WHO. The Translational Pathology Shared Resource is supported by NCI/NIH Cancer Center Support Grant 5P30 CA68485-19 and the Vanderbilt Mouse Metabolic Phenotyping Center Grant 2 U24 DK059637-16. Lin Zhong from the Vanderbilt University Cardiology Physiology Core to assist with Echocardiogram.

Conflicts of Interest: J.P.A. reports consulting, advisory roles, and/or stocks/ownership for Achelois, Apricity Health, BioAlta, Codiak BioSciences, Dragonfly Therapeutics, Forty-Seven Inc., Hummingbird, ImaginAb, Jounce Therapeutics, Lava Therapeutics, Lytix Biopharma, Marker Therapeutics, BioNTx, and Polaris. L.L. serves on advisory boards for Servier. S.C.W. and J.P.A. are inventors of a patent application submitted by The University of Texas MD Anderson Cancer Center related to a genetic mouse model of immune checkpoint blockade induced immune-related adverse events. S.C.W. is currently an employee of Spotlight Therapeutics. E.M.W has ownership interest in Pathogenesis, LLC. W.C.M. was supported by funding from the Niels Stensen Fellowship and the Netherlands Heart Institute. D.B.J serves on advisory boards for Array Biopharma, BMS, Merck, Novartis; research funding from BMS and Incyte. J.E.S serves on advisory boards for BMS. J.E.S, D.B.J and J.J.M are inventors of a patent application submitted by The Assistance Publique – Hopitaux de Paris related to abatacept for the treatment of immune-related adverse events associated with immune checkpoint inhibitors.

References

1. Larkin J, Chiarion-Sileni V, Gonzalez R, Grob JJ, Cowey CL, Lao CD, et al. Combined Nivolumab and Ipilimumab or Monotherapy in Untreated Melanoma. N Engl J Med [Internet]. 2015;373:23–34. Available from: http://www.ncbi.nlm.nih.gov/pubmed/26027431 [PubMed: 26027431]
2. Motzer RJ, Tannir NM, McDermott DF, Aren Frontera O, Melichar B, Choueiri TK, et al. Nivolumab plus Ipilimumab versus Sunitinib in Advanced Renal-Cell Carcinoma. N Engl J Med [Internet]. 2018/03/22. 2018;378:1277–90. Available from: https://www.ncbi.nlm.nih.gov/pubmed/29562145 [PubMed: 29562145]
3. Overman MJ, Lonardi S, Wong KYM, Lenz HJ, Gelsomino F, Aglietta M, et al. Durable Clinical Benefit With Nivolumab Plus Ipilimumab in DNA Mismatch Repair-Deficient/Microsatellite Instability-High Metastatic Colorectal Cancer. J Clin Oncol [Internet]. 2018/01/23. 2018;36:773–9. Available from: https://www.ncbi.nlm.nih.gov/pubmed/29355075 [PubMed: 29355075]
4. Postow MA, Chesney J, Pavlick AC, Robert C, Grossmann K, McDermott D, et al. Nivolumab and ipilimumab versus ipilimumab in untreated melanoma. N Engl J Med [Internet]. 2015;372:2006–17. Available from: http://www.ncbi.nlm.nih.gov/pubmed/25891304 [PubMed: 25891304]
5. Wolchok JD, Kluger H, Callahan MK, Postow MA, Rizvi NA, Lesokhin AM, et al. Nivolumab plus ipilimumab in advanced melanoma. N Engl J Med [Internet]. 2013;369:122–33. Available from: http://www.ncbi.nlm.nih.gov/pubmed/23724867 [PubMed: 23724867]
6. Barroso-Sousa R, Barry WT, Garrido-Castro AC, Hodi FS, Min L, Krop IE, et al. Incidence of Endocrine Dysfunction Following the Use of Different Immune Checkpoint Inhibitor Regimens: A Systematic Review and Meta-analysis. JAMA Oncol [Internet]. 2017/10/04. 2018;4:173–82. Available from: https://www.ncbi.nlm.nih.gov/pubmed/28973656 [PubMed: 28973656]
7. Johnson DB, Balko JM, Compton ML, Chalkias S, Gorham J, Xu Y, et al. Fulminant Myocarditis with Combination Immune Checkpoint Blockade. N Engl J Med [Internet]. 2016;375:1749–55. Available from: http://www.ncbi.nlm.nih.gov/pubmed/27806233 [PubMed: 27806233]
8. Moslehi JJ, Salem JE, Sosman JA, Lebrun-Vignes B, Johnson DB. Increased reporting of fatal immune checkpoint inhibitor-associated myocarditis. Lancet 2018;391(10124):933 doi 10.1016/S0140-6736(18)30533-6.
9. Sznol M, Ferrucci PF, Hogg D, Atkins MB, Wolter P, Guidoboni M, et al. Pooled Analysis Safety Profile of Nivolumab and Ipilimumab Combination Therapy in Patients With Advanced Melanoma. J Clin Oncol [Internet]. 2017;35:3815–22. Available from: https://www.ncbi.nlm.nih.gov/pubmed/28915085 [PubMed: 28915085]
10. Palaskas N, Lopez-Mattei J, Durand JB, Iliescu C, Deswal A. Immune Checkpoint Inhibitor Myocarditis: Pathophysiological Characteristics, Diagnosis, and Treatment. J Am Heart Assoc. 2020;9.
11. Zamami Y, Niimura T, Okada N, Koyama T, Fukushima K, Izawa-Ishizawa Y, et al. Factors Associated with Immune Checkpoint Inhibitor-Related Myocarditis. JAMA Oncol. 2019;5:1635–7.

12. Valpione S, Pasquali S, Campana LG, Piccin L, Mocellin S, Pigozzo J, et al. Sex and interleukin-6 are prognostic factors for autoimmune toxicity following treatment with anti-CTLA4 blockade. J Transl Med. 2018;16.
13. Johnson DB, Balko JM, Compton ML, Chalkias S, Gorham J, Xu Y, et al. Fulminant myocarditis with combination immune checkpoint blockade. N Engl J Med. 2016;375:1749–55. [PubMed: 27806233]
14. Salem JE, Manouchehri A, Moey M, Lebrun-Vignes B, Bastarache L, Pariente A, et al. Cardiovascular toxicities associated with immune checkpoint inhibitors: an observational, retrospective, pharmacovigilance study. Lancet Oncol. 2018;19:1579–89. [PubMed: 30442497]
15. Lucas JA, Menke J, Rabacal WA, Schoen FJ, Sharpe AH, Kelley VR. Programmed death ligand 1 regulates a critical checkpoint for autoimmune myocarditis and pneumonitis in MRL mice. J Immunol 2008;181(4):2513–21 doi 10.4049/jimmunol.181.4.2513. [PubMed: 18684942]
16. Wang J, Okazaki IM, Yoshida T, Chikuma S, Kato Y, Nakaki F, et al. PD-1 deficiency results in the development of fatal myocarditis in MRL mice. Int Immunol. 2010;22:443–52. [PubMed: 20410257]
17. Wei SC, Duffy CR, Allison JP. Fundamental Mechanisms of Immune Checkpoint Blockade Therapy. Cancer Discov 2018;8(9):1069–86 doi 10.1158/2159-8290.CD-18-0367. [PubMed: 30115704]
18. Chen L, Flies DB. Molecular mechanisms of T cell co-stimulation and co-inhibition. Nat Rev Immunol [Internet]. 2013;13:227–42. Available from: http://www.ncbi.nlm.nih.gov/pubmed/23470321 [PubMed: 23470321]
19. Parry RV, Chemnitz JM, Frauwirth KA, Lanfranco AR, Braunstein I, Kobayashi SV, et al. CTLA-4 and PD-1 receptors inhibit T-cell activation by distinct mechanisms. Mol Cell Biol [Internet]. 2005;25:9543–53. Available from: http://www.ncbi.nlm.nih.gov/pubmed/16227604 [PubMed: 16227604]
20. Chambers CA, Cado D, Truong T, Allison JP. Thymocyte development is normal in CTLA-4-deficient mice. Proc Natl Acad Sci U S A [Internet]. 1997;94:9296–301. Available from: http://www.ncbi.nlm.nih.gov/pubmed/9256476 [PubMed: 9256476]
21. Keir ME, Freeman GJ, Sharpe AH. PD-1 regulates self-reactive CD8+ T cell responses to antigen in lymph nodes and tissues. J Immunol [Internet]. 2007;179:5064–70. Available from: http://www.ncbi.nlm.nih.gov/pubmed/17911591 [PubMed: 17911591]
22. Tivol EA, Borriello F, Schweitzer AN, Lynch WP, Bluestone JA, Sharpe AH. Loss of CTLA-4 leads to massive lymphoproliferation and fatal multiorgan tissue destruction, revealing a critical negative regulatory role of CTLA-4. Immunity [Internet]. 1995;3:541–7. Available from: http://www.ncbi.nlm.nih.gov/pubmed/7584144 [PubMed: 7584144]
23. Waterhouse P, Penninger JM, Timms E, Wakeham A, Shahinian A, Lee KP, et al. Lymphoproliferative disorders with early lethality in mice deficient in Ctla-4. Science (80-) [Internet]. 1995;270:985–8. Available from: http://www.ncbi.nlm.nih.gov/pubmed/7481803
24. Wei SC, Sharma R, Anang NAAS, Levine JH, Zhao Y, Mancuso JJ, et al. Negative Co-stimulation Constrains T Cell Differentiation by Imposing Boundaries on Possible Cell States. Immunity. 2019;50:1084–1098.e10. [PubMed: 30926234]
25. Nishimura H, Okazaki T, Tanaka Y, Nakatani K, Hara M, Matsumori A, et al. Autoimmune dilated cardiomyopathy in PD-1 receptor-deficient mice. Science (80-) [Internet]. 2001;291:319–22. Available from: http://www.ncbi.nlm.nih.gov/pubmed/11209085
26. Nishimura H, Nose M, Hiai H, Minato N, Honjo T. Development of lupus-like autoimmune diseases by disruption of the PD-1 gene encoding an ITIM motif-carrying immunoreceptor. Immunity [Internet]. 1999;11:141–51. Available from: http://www.ncbi.nlm.nih.gov/pubmed/10485649 [PubMed: 10485649]
27. Mahmood SS, Fradley MG, Cohen JV., Nohria A, Reynolds KL, Heinzerling LM, et al. Myocarditis in Patients Treated With Immune Checkpoint Inhibitors. J Am Coll Cardiol. 2018;71:1755–64. [PubMed: 29567210]
28. Escudier M, Cautela J, Malissen N, Ancedy Y, Orabona M, Pinto J, et al. Clinical Features, Management, and Outcomes of Immune Checkpoint Inhibitor-Related Cardiotoxicity. Circulation 2017;136(21):2085–7 doi 10.1161/CIRCULATIONAHA.117.030571 [PubMed: 29158217]

29. Salem JE, Allenbach Y, Kerneis M. Abatacept for severe immune checkpoint inhibitor–associated myocarditis. N Engl J Med [Internet]. Massachusetts Medical Society; 2019;380:2377–9. Available from: 10.1056/NEJMc1901677 [PubMed: 31189043]
30. Kamphorst AO, Wieland A, Nasti T, Yang S, Zhang R, Barber DL, et al. Rescue of exhausted CD8 T cells by PD-1-targeted therapies is CD28-dependent. Science (80-) [Internet]. 2017;355:1423–7. Available from: http://www.ncbi.nlm.nih.gov/pubmed/28280249
31. Okazaki T, Tanaka Y, Nishio R, Mitsuiye T, Mizoguchi A, Wang J, et al. Autoantibodies against cardiac troponin I are responsible for dilated cardiomyopathy in PD-1-deficient mice. Nat Med [Internet]. 2003;9:1477–83. Available from: http://www.ncbi.nlm.nih.gov/pubmed/14595408 [PubMed: 14595408]
32. Elamm C, Fairweather D, Cooper LT. Pathogenesis and diagnosis of myocarditis. Heart 2012;98(11):835–40 doi 10.1136/heartjnl-2012–301686. [PubMed: 22442199]
33. Legoux FP, Lim JB, Cauley AW, Dikiy S, Ertelt J, Mariani TJ, et al. CD4+ T Cell Tolerance to Tissue-Restricted Self Antigens Is Mediated by Antigen-Specific Regulatory T Cells Rather Than Deletion. Immunity [Internet]. 2015/11/18. 2015;43:896–908. Available from: https://www.ncbi.nlm.nih.gov/pubmed/26572061 [PubMed: 26572061]
34. Kuehn HS, Ouyang W, Lo B, Deenick EK, Niemela JE, Avery DT, et al. Immune dysregulation in human subjects with heterozygous germline mutations in CTLA4. Science (80-) [Internet]. 2014;345:1623–7. Available from: http://www.ncbi.nlm.nih.gov/pubmed/25213377
35. Schubert D, Bode C, Kenefeck R, Hou TZ, Wing JB, Kennedy A, et al. Autosomal dominant immune dysregulation syndrome in humans with CTLA4 mutations. Nat Med [Internet]. 2014;20:1410–6. Available from: http://www.ncbi.nlm.nih.gov/pubmed/25329329 [PubMed: 25329329]
36. Schwab C, Gabrysch A, Olbrich P, Patino V, Warnatz K, Wolff D, et al. Phenotype, penetrance, and treatment of 133 cytotoxic T-lymphocyte antigen 4-insufficient subjects. J Allergy Clin Immunol [Internet]. 2018/05/08. 2018; Available from: https://www.ncbi.nlm.nih.gov/pubmed/29729943
37. Bogue MA, Grubb SC, Walton DO, Philip VM, Kolishovski G, Stearns T, et al. Mouse Phenome Database: an integrative database and analysis suite for curated empirical phenotype data from laboratory mice. Nucleic Acids Res [Internet]. 2017/11/15. 2018;46:D843–50. Available from: https://www.ncbi.nlm.nih.gov/pubmed/29136208 [PubMed: 29136208]
38. Bankhead P, Loughrey MB, Fernández JA, Dombrowski Y, McArt DG, Dunne PD, et al. QuPath: Open source software for digital pathology image analysis. Sci Rep. 2017;7.
39. Kallikourdis M, Martini E, Carullo P, Sardi C, Roselli G, Greco CM, et al. T cell costimulation blockade blunts pressure overload-induced heart failure. Nat Commun. 2017;8.
40. Lindquist M VigiBase, the WHO Global ICSR Database System: Basic facts. Drug Inf J. 2008;42:409–19.

Statement of Significance

We provide a preclinical model of immune checkpoint inhibitor (ICI)-associated myocarditis which recapitulates this clinical syndrome. Using this model, we demonstrate that CTLA-4 and PD-1 (ICI targets) functionally interact for myocarditis development and that intervention with CTLA-4-Ig (abatacept) attenuates myocarditis, providing mechanistic rationale and preclinical support for therapeutic clinical studies.

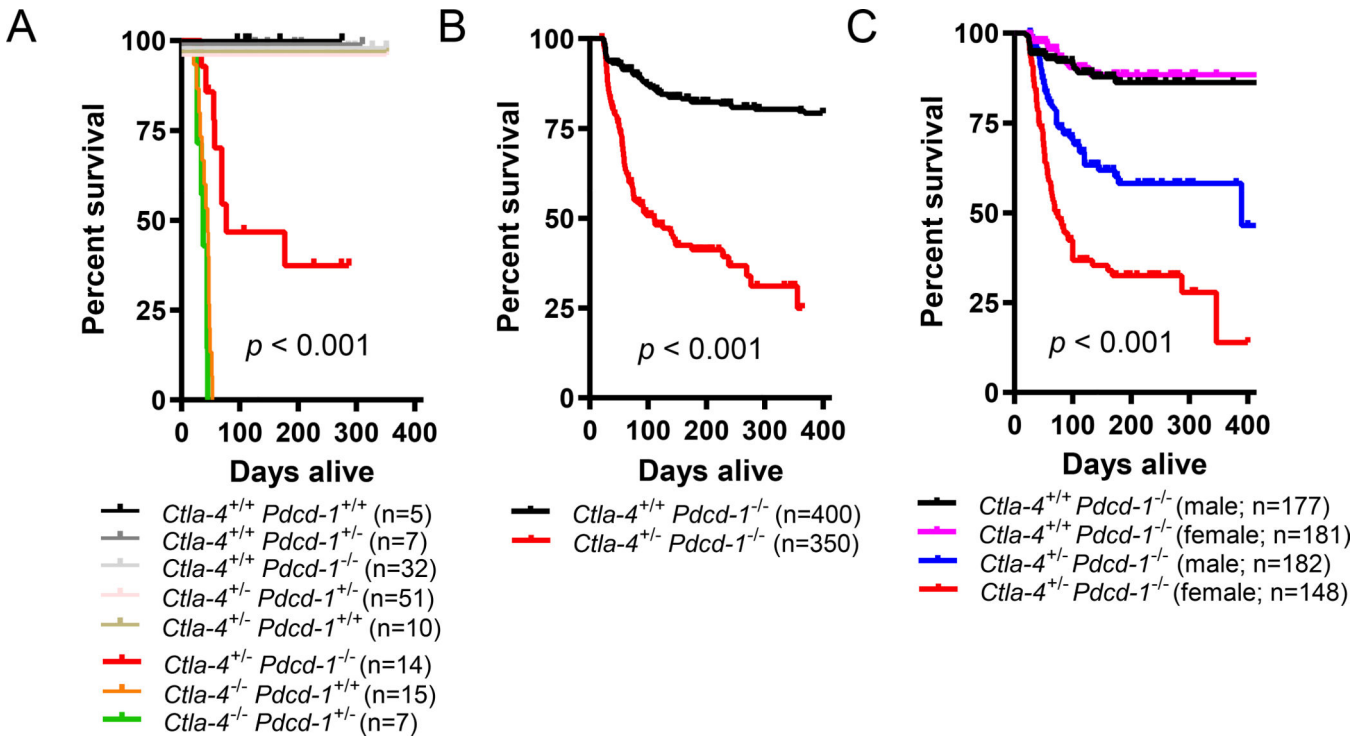

Figure 1: Lethal haploinsufficiency of *Ctla4* in the genetic absence of *Pdcd1*.

A) Kaplan-Meier survival curve of transgenic *C57BL6/J* mice harboring *Ctla4* and *Pdcd1* knockout alleles. Mice were derived from an intercross of $Ctla4^{+/-}$ $Pdcd1^{+/-}$ mice in which *Pdcd1* and *Ctla4* loss of function alleles are in *trans*. Individual mice were censored if used for breeding or alive at the time of data analysis. Death events were defined as mice found dead or identified by veterinary staff as requiring euthanasia. P-value represents the result of the Mantel-Cox Log-rank test. B) Kaplan-Meier survival curve of $Ctla4^{+/-}$ $Pdcd1^{-/-}$ (n = 350) and littermate $Ctla4^{+/+}$ $Pdcd1^{-/-}$ (n = 400) mice derived from a $Ctla4^{+/-}$ $Pdcd1^{-/-}$ by $Ctla4^{+/+}$ $Pdcd1^{-/-}$ breeding cross performed at the Vanderbilt University Medical Center (VUMC) vivarium. P-value represents the result of the Mantel-Cox Log-rank test. C) Kaplan-Meier survival curve of $Ctla4^{+/-}$ $Pdcd1^{-/-}$ and littermate $Ctla4^{+/+}$ $Pdcd1^{-/-}$ mice stratified by sex. Data are pooled from studies performed at MDACC and VUMC. P-value represents the result of the Mantel-Cox Log-rank test.

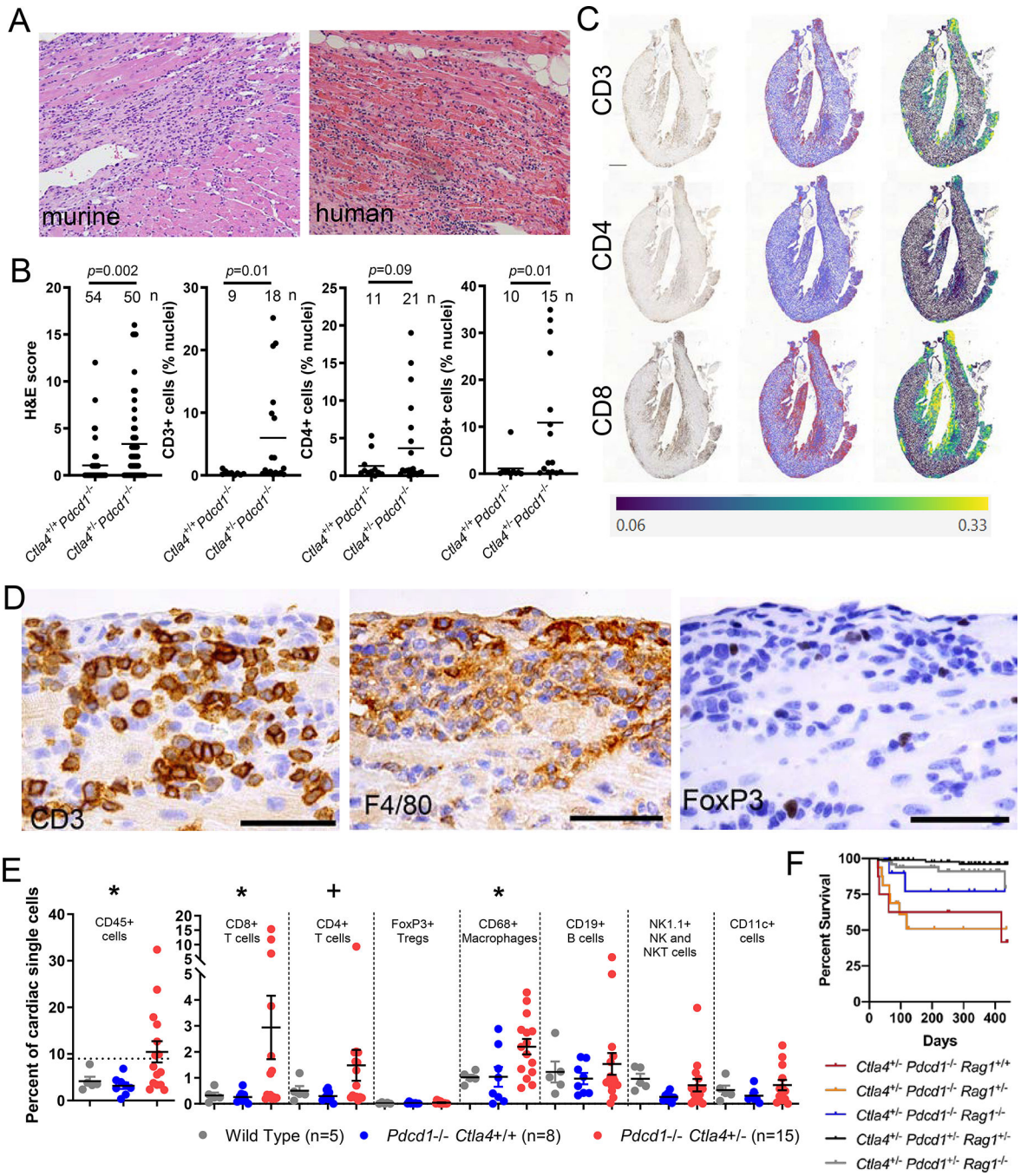

Figure 2: *Ctla4*$^{+/-}$ *Pdcd1*$^{-/-}$ mice present with cardiac immune infiltration.

A) 20X H&E images of lymphocytic infiltration in *Ctla4*$^{+/-}$ *Pdcd1*$^{-/-}$ mouse (left) and human (right; autopsy sample from myocardium of a patient that had complete heart block and ventricular tachycardia following ICI treatment.) **B)** Quantification of lymphoid infiltrate scores from H&E stained heart tissue (see methods) and frequency of CD3, CD4, and CD8+ cells (IHC) as a fraction of total nucleated cells. P-value represents result of unpaired Student's T-test with Welch's correction. **C)** Representative images of CD3, CD4, and CD8 immunohistochemistry (right) stained heart tissue sections from female *Ctla4*$^{+/-}$

Pdcd1$^{-/-}$ mice. Left panels: IHC; Middle panels: segmentation with red=positive and blue=negative cells; right panels: positive cell density (blue=low, green=intermediate, yellow=high). Heatmap values represent arbitrary density units. **D)** Representative images of additional immunohistochemistry (CD3, F4/80+ macrophages and Foxp3+ Tregs) stained heart tissue from *Ctla4*$^{+/-}$ *Pdcd1*$^{-/-}$ mice. **E)** Flow cytometry analysis of immune populations in murine cardiac tissue. *ANOVA $p<0.05$; +ANOVA $p<0.10$. Dashed line at 9% CD45+ cells was used as a stratification factor for 'high' versus 'low' infiltrated samples in Fig. 3. See also Supplemental Figure 9A for analyses as percentage of total CD45+ immune cells. **F)** Kaplan-Meier survival curve of *Ctla4*$^{+/-}$ *Pdcd1*$^{-/-}$ *Rag1*$^{-/-}$ (n=10) and littermate RAG1 competent *Ctla4*$^{+/-}$ *Pdcd1*$^{-/-}$ *Rag1*$^{+/+}$ and *Ctla4*$^{+/-}$ *Pdcd1*$^{-/-}$ *Rag1*$^{+/-}$ mice (n=8 and 16, respectively). Littermate *Ctla4*$^{+/-}$ *Pdcd1*$^{+/-}$ *Rag1*$^{+/-}$ and *Ctla4*$^{+/-}$ *Pdcd1*$^{+/-}$ *Rag1*$^{-/-}$ mice are also displayed (n=99 and 51, respectively).

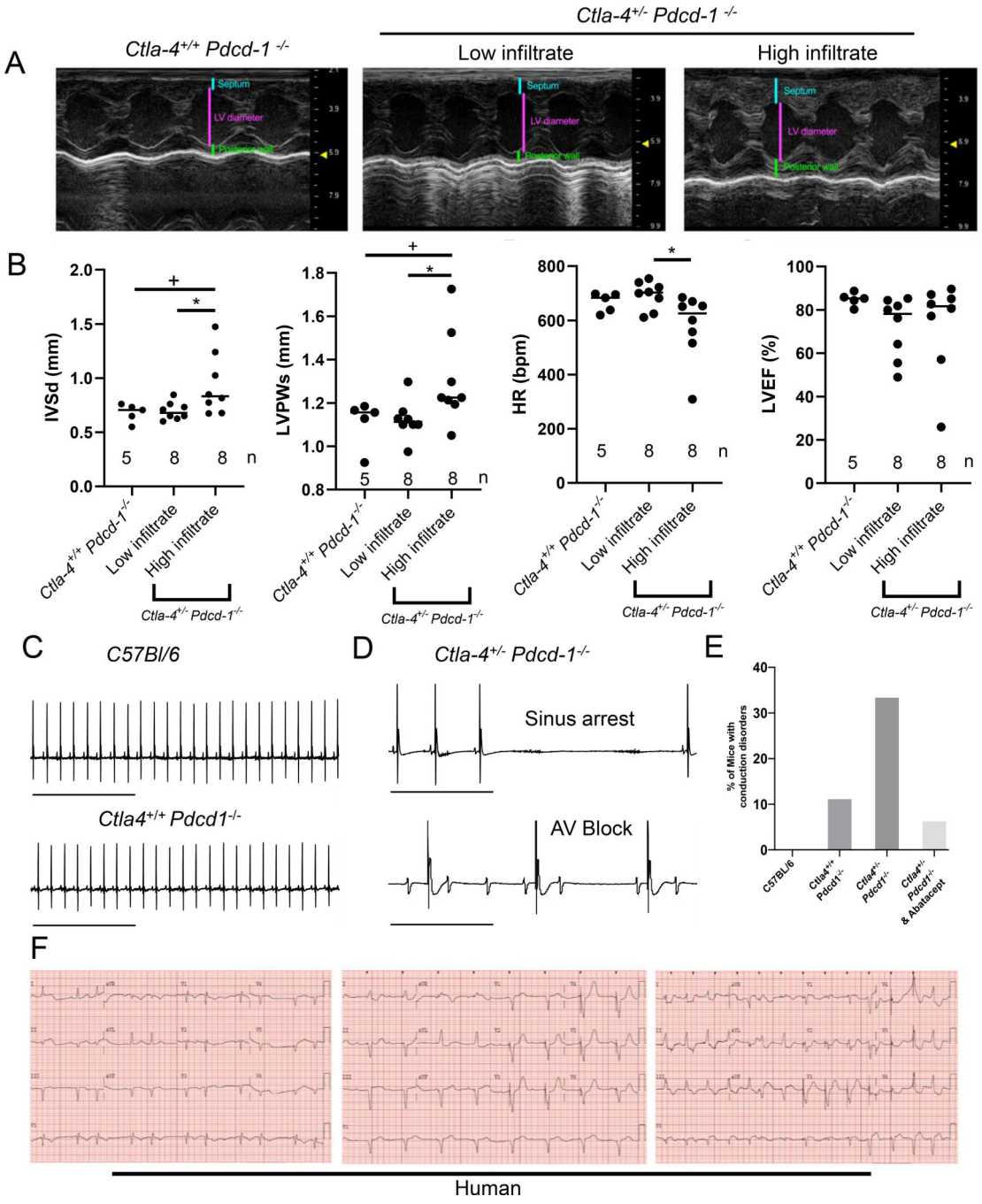

Figure 3: Functional cardiologic manifestations of autoimmune myocarditis in *Ctla4*$^{+/-}$ *Pdcd1*$^{-/-}$ mice are similar to those occurring in patients.

A) Representative echocardiograms from *Ctla4*$^{+/+}$ *Pdcd1*$^{-/-}$, low immune infiltrate (<9% CD45+ cells) *Ctla4*$^{+/-}$ *Pdcd1*$^{-/-}$, and high immune infiltrate (≥9% CD45+ cells) *Ctla4*$^{+/-}$ *Pdcd1*$^{-/-}$ mice. **B**) Quantification of cardiac properties and output in *Ctla4*$^{+/+}$ *Pdcd1*$^{-/-}$, low immune infiltrate (<9%) *Ctla4*$^{+/-}$ *Pdcd1*$^{-/-}$, and high immune infiltrate (≥9%) *Ctla4*$^{+/-}$ *Pdcd1*$^{-/-}$ mice. LVPWs: Left Ventricular Posterior Wall (systole); IVSd: Interventricular Septum (diastole); HR: Heart Rate; LVEF: Left Ventricular Ejection Fraction *p < 0.05 and

$^{+}$p <0.10 Kruskal-Wallis test with Dunn's multiple comparison. **C**) Representative electrocardiography records from wild-type *C57BL6/J* (left panel) and *Ctla4*$^{+/+}$ *Pdcd1*$^{-/-}$ mice demonstrating normal sinus rhythm. **D)** Representative electrocardiography records from *Ctla4*$^{+/-}$ *Pdcd1*$^{-/-}$ mice demonstrating sinus arrest and AV block. **E)** Percent of mice in wild-type *C57/BL6, Ctla4*$^{+/+}$ *Pdcd1*$^{-/-}$ *, and Ctla4*$^{+/-}$ *Pdcd1*$^{-/-}$ genotypes or *Ctla4*$^{+/-}$ *Pdcd1*$^{-/-}$ treated with abatacept demonstrating observed conduction disorders. **F**) Representative electrocardiograms (ECG) from 3 patients with ICI-associated myocarditis. All patients were treated with ipilimumab and nivolumab with clinical presentation within 2 weeks of dose with ECG on admission. There is 3:2 conduction block and QRS widening (left panel), third degree heart block with ventricular pacing (middle panel), and ventricular pacing competing with an accelerated ventricular rhythm (right panel).

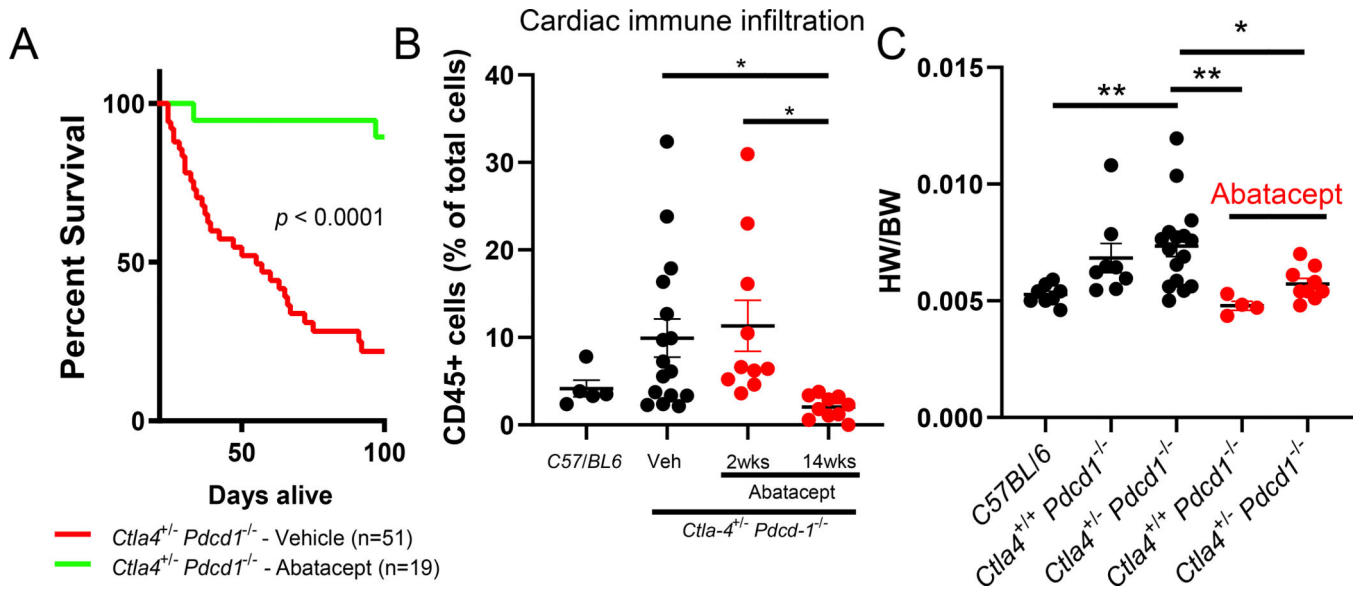

Figure 4: Modulation of CTLA-4 and PD-1 T cell negative costimulation leads to functional changes in cardiac pathology.

A) Kaplan-Meier survival curve of female *Ctla4*$^{+/-}$ *Pdcd1*$^{-/-}$ mice treated with either vehicle (n=51) or abatacept (n = 19). P-value represents the outcome of the log-rank test. **B**) Infiltration of CD45+ immune cells assessed by flow cytometry analysis of heart tissue from female *Ctla4*$^{+/+}$ *Pdcd1*$^{-/-}$ and *Ctla4*$^{+/-}$ *Pdcd1*$^{-/-}$ mice with and without abatacept treatment. *, p < 0.05 ANOVA with Tukey's multiple testing correction. **C**) Heart-weight/body-weight (HW/BW) ratio of female *Ctla4*$^{+/+}$ *Pdcd1*$^{-/-}$ and *Ctla4*$^{+/-}$ *Pdcd1*$^{-/-}$ mice with and without abatacept treatment. ** p < 0.01; *p<0.05 ANOVA with Dunn's multiple testing correction comparing all groups to *Ctla-4*$^{+/-}$ *Pdcd-1*$^{-/-}$ control mice.